catalysts

MDPI

Review

Insights into the Influence of Key Preparation Parameters on the Performance of MoS_2/Graphene Oxide Composites as Active Materials in Supercapacitors

Catalin Alexandru Salagean [1,2], Codrut Costinas [2], Liviu Cosmin Cotet [1,3] and Lucian Baia [1,2,4,*]

1 Laboratory for Advanced Materials and Applied Technologies, Institute for Research, Development and Innovation in Applied Natural Sciences, Babeș-Bolyai University, Fantanele 30, RO-400294 Cluj-Napoca, Romania; catalin.salagean@ubbcluj.ro (C.A.S.); cosmin.cotet@ubbcluj.ro (L.C.C.)
2 Faculty of Physics, Babeș-Bolyai University, M. Kogalniceanu 1, RO-400084 Cluj-Napoca, Romania; codrut98@gmail.com
3 Faculty of Chemistry and Chemical Engineering, Babeș-Bolyai University, Arany Janos 11, RO-400024 Cluj-Napoca, Romania
4 Centre of Nanostructured Materials and Bio-Nano Interfaces, Institute for Interdisciplinary Research on Bio-Nano-Sciences, Babeș-Bolyai University, Treboniu Laurian 42, RO-400271 Cluj-Napoca, Romania
* Correspondence: lucian.baia@ubbcluj.ro

Abstract: Advances in energy storage and energy conversion play an essential role nowadays because the energy demands are becoming greater than ever. To overcome the actual performances of the materials used to build supercapacitors, a combination of transition metal dichalcogenides (TMDCs) and graphene oxide (GO) or reduced graphene oxide (rGO) as graphene-based structures are often studied for their excellent properties, such as high specific area and good electrical conductivity. Nevertheless, synthesis pathways and parameters play key roles in obtaining better materials as components for supercapacitors with higher technical performances. Driven by the desire to understand the influence of the structural and morphological particularities on the performances of supercapacitors based on MoS_2/graphene oxide (GO) composites, a survey of the literature was performed by pointing out the alterations induced by different synthesis pathways and key parameters to the above-mentioned particularities.

Keywords: supercapacitors; hydrothermal; MoS_2; graphene oxide; parameters

Citation: Salagean, C.A.; Costinas, C.; Cotet, L.C.; Baia, L. Insights into the Influence of Key Preparation Parameters on the Performance of MoS_2/Graphene Oxide Composites as Active Materials in Supercapacitors. *Catalysts* **2021**, *11*, 1553. https://doi.org/10.3390/catal11121553

Academic Editors: Paloma Fernández Sánchez, Ana Urbieta, María Eugenia Rabanal Jiménez and Olivera Milošević

Received: 12 November 2021
Accepted: 3 December 2021
Published: 20 December 2021

1. Introduction

In the last few years, due to the advances in the current technologies such as electric/hybrid powered vehicles and day to day electronics, there has grown a high demand for energy storage systems with high power and energy density combined with a long lifespan. Currently, batteries are capable of high energy density, but the charging process is very slow. On the other hand, supercapacitors can deliver high power density with a much higher lifespan but fall short in terms of energy density [1]. Despite the progress made in the last period, the scientific community has a strong interest in developing various techniques and materials to advance energy storage system technologies [2].

Due to their high-power density, supercapacitors and their high charge/discharge rate, long cycle life (>1,000,000 cycles) and simple operation mode, are to be considered one of the most promising energy storage units [3]. The advantage of supercapacitors related to batteries is that charging is not limited by the diffusion of ions in the material, so they could supplement or even replace batteries when high power is needed to be delivered [4].

In general, depending on the energy storage types, the involved technology consists of three types of supercapacitors [5–7], as presented in Figure 1.

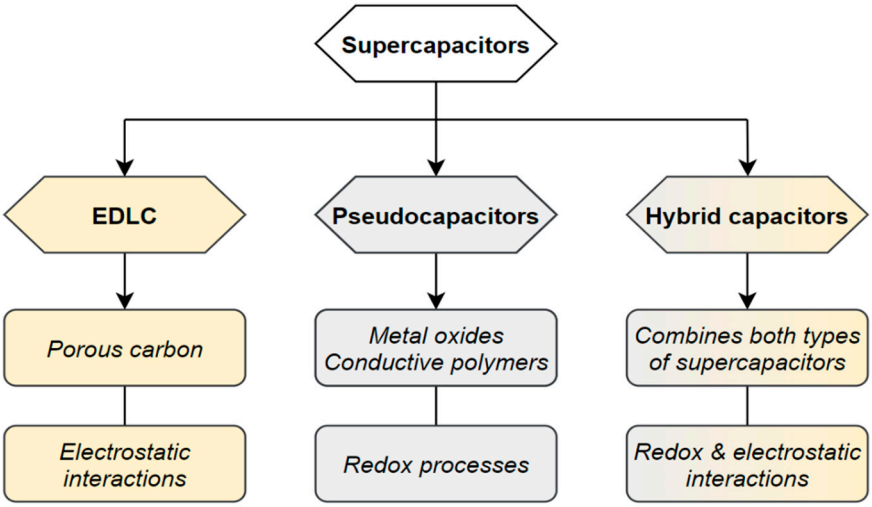

Figure 1. Classification of supercapacitors based on their energy storage mechanism, specifying the active materials and the processes involved.

The first type is the electrochemical double-layer capacitor (EDLC), which uses mostly porous carbon with a high specific surface area as the main active material. The electrostatic interactions between the electrolyte ions and electrode surface charges, are the basis for EDLCs, which operate as an "electrical sponge" that adsorbs and desorbs the ions in a charge–discharge mechanism. The second type of supercapacitors are represented by the pseudo-capacitor, which is mainly based on electro-chemical pseudo-capacitance provided by the redox reactions occurring at the electrolyte–active material interface, which is made up of various oxides and conductive polymers. Another type is the hybrid supercapacitor, which combines the two types of energy storage. The hybrid supercapacitors have come to life due to the desire for increased performances. Their functionality is based on the coupling mechanism between EDLCs and pseudo-capacitors, which are meant to increase the power output and cyclability [4,8].

Part of the reported literature [9,10] presents activated carbon with good capacitance (varying from 100 to 200 $F \cdot g^{-1}$) as the most commonly utilized material for supercapacitor electrodes, mainly due to their great specific surface area, high electrical conductivity, low production cost, etc. Significant research effort has been placed in the last few decades into the improvement of their performance by using composites such as conductive polymers and metallic oxides [11–13]. Moreover, nitrogen-enriched activated carbon was studied and its impact on the porosity of carbons and the dependence of capacity on the chemistry of surface groups were discussed [14]. Furthermore, in order to get higher energy density, various designs have been considered such as asymmetric capacitor systems consisting of different electrodes like (activated carbon)/$LiMn_2O_4$ [15,16], activated carbon/graphene/MnO_2, [17] Na_xMnO_2/N-(rGO) [18], and also symmetric supercapacitors, which have similar electrodes, such as MoS_2-rGO with poly(3,4-ehylenedioxythiophene) [5], and were tested in energy storage applications. Other intriguing approaches were reported about the composites based on graphene materials and MoS_2 [19]. These combinations represent excellent choices for the use of novel electrode materials in terms of energy storage technologies, due to their good characteristics, such as a high specific surface area, and thermal stability.

Graphene, GO and rGO, are usually obtained by chemical vapor deposition (CVD), mechanical and/or oxidative exfoliation of the graphite followed by reduction techniques (in the case of rGO, the unreduced form being GO), and are generally termed as graphene materials. These materials have excellent features such as large specific area and are considered suitable options for obtaining electrode materials in supercapacitors [20–22]. However, graphene structures, taken as an individual component, limit the supercapacitor performances. A good strategy to overcome this drawback is to combine graphene materials

with various components. In this respect, it is worth mentioning the use of transition-metal dichalcogenides (TMDCs) that gained a lot of interest in the past few years due to their physical and chemical properties [23–25]. For example, due to their large specific area and their rich redox chemistry, these structures are thought to have significant potential as supercapacitor electrode materials.

Besides this, many research groups [26–30] found that another promising material for supercapacitor construction is molybdenum disulfide (MoS_2). Because MoS_2 is easily intercalated by other compounds and has a great theoretical capacitance ($\pm 1000\ F \cdot g^{-1}$), it can be used to build layered electrode materials for the construction of supercapacitors [31]. These are built up from a graphite-like layered structure stacked by covalently bonded S-Mo-S layers, and bonded by weak van der Waals forces [32,33].

Taking into account the above presented information, it becomes obvious that there is a real interest to understand the synthesis pathways and parameters that lead to the alteration of the morphological, structural and surface particularities of the MoS_2-GO composites from the perspective of the improvement of supercapacitor performances. In this respect, this review proposes, based on a comprehensive survey of the literature, to bring more light to these above-mentioned aspects by presenting the existent correlations between the obtaining procedures, properties and the achieved performances in the case of MoS_2 nanostructures and MoS_2-GO composites.

At the beginning of the review will be presented an overview of the synthesis methods and parameters involved in the obtaining of MoS_2 nanostructures. Further on, the effects of each preparation parameter on the structure, morphology, and surface particularities of MoS_2/MoS_2-rGO composites will be discussed, with an emphasis on the essential properties required for designing efficient supercapacitors. Several promising electrode material results in terms of specific capacitance and cycle stability will be further pointed out. A list of these achievements based on certain essential criteria for supercapacitor applications, such as specific capacitance and cycle stability of electrode materials, and their ranking in order of performance, is also presented.

2. Synthesis Methods for MoS_2/MoS_2 Composites

The synthesis methods of molybdenum disulfide can be divided into two major categories, such as bottom-up and top-down [34,35], as depicted in Figure 2.

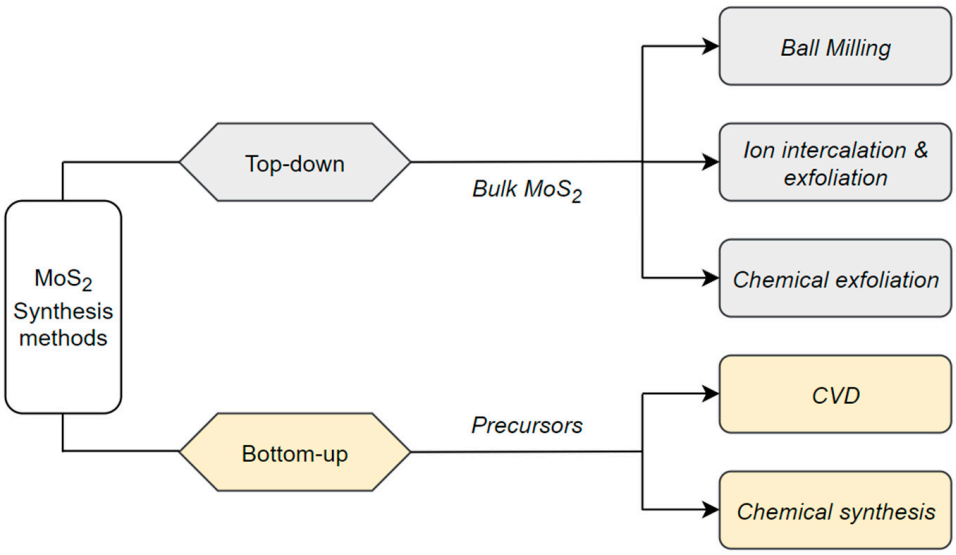

Figure 2. MoS_2 synthesis pathways.

Each of them uses different techniques and, as expected, has advantages and disadvantages. In the first category, the chemical exfoliation, mechanical cleavage and ball milling is highlighted. In the second one chemical vapor deposition (CVD), and wet chemical synthesis, which is based on hydrothermal/solvothermal processes, are described.

The synthesis pathways are chosen depending on the targeted properties of the final MoS_2 product; however, the most commonly used preparation method for MoS_2 composites is the hydrothermal technique. One of the parameters that influences the morphology and properties of the composites is the reaction time of the hydrothermal process that affects directly the morphology of MoS_2, which can vary from nanosheets, or nanospheres to flower-like hierarchical structures [36,37]. Another element that influences the synthesis is the reducing agent type, which is also the sulfur source. Taking this into account, the molybdenum species, as well as thiourea, sodium thiosulfate, L-cysteine and thio-acetamide, which act as sulfur sources by contributing to the sulfuration of the molybdenum species, were investigated [36]. Surfactants also play a decisive role in the synthesis of MoS_2 composites because they act as a mediator between the two precursors and control the pore-size, ultimately affecting the specific surface area and the conductivity [6,38–40]. Moreover, the binding agent can also influence the conductivity of the active material, thereby influencing the final specific capacitance of the cell. Another parameter worth taking into account is the molar ratios between the Mo and S precursors, which affects directly the crystallinity of the composite [28]. One of the most common routes used to obtain MoS_2 composites is the hydrothermal approach [28,29,36]. The hydrothermal method facilitates the formation of hierarchical porous structures that can improve the performances of supercapacitors by providing active unsaturated sulfur sites. Moreover, the addition of graphene materials can increase the composite's electrical conductivity as a result of the rGO formation after hydrothermal treatment is applied, which turns this type of carbonic structure into a strong competitor for the novel electrode materials for energy storage cells [6,37,41].

2.1. Top-Down Methods for MoS_2 Synthesis

From the top-down pathways, two common methods are discussed in this study, namely the chemical exfoliation and ball milling.

Chemical exfoliation is based on breaking the weak van der Waals forces between the MoS_2 (S-Mo-S) layers (process assisted by sonication), thus facilitating the liquid-based exfoliation processes [42]. It is worth mentioning that in order to obtain MoS_2 nanosheets by chemical exfoliation one can choose the organolithium method, in which the medium is a mixture with n-butyl lithium solutions or by choosing some organic solvents [7,42].

The exfoliation of semiconducting 2H molybdenum disulfide crystalline phase is based on intercalating Li ions after using organolithium compounds, which results in the formation of single layer MoS_2 nanosheets in the form of Li_xMoS_2. Afterwards, the molybdenum disulfide intercalated with lithium ions will interact with water during sonication, producing a MoS_2 dispersion.

Another aspect that needs to be discussed here is the transition of MoS_2 from the semiconducting crystalline 2H phase to the metallic 1T crystalline phase with defects in the lattice. In some cases, defects created by the transition to 1T metallic phase improves the electrochemical performances of the active material by generating additional sulfur active sites and affecting the band structure of the composite [43], giving it an advantage over the semiconducting 2H phase. Furthermore, the electrical conductivity of the 1T metallic phase is seven-orders of magnitude greater than that of the 2H-MoS_2 phase [37,44]. MoS_2 crystalline phases are depicted in Figure 3.

Another procedure for liquid phase exfoliation of molybdenum disulfide is sonication assisted by organic solvents such as N-methyl-2-pyrrolidone (NMP). MoS_2 can be obtained easily using NMP without the use of any surfactants. Moreover, the surface tension of the TMDCs should closely match the solvent's surface tension [45]. Although surfactant-assisted chemical exfoliation using organic solvents prevents the aggregation of MoS_2

nanosheets by stabilizing the dispersion [46], it does not impact the structure of the material by creating phase changes like the one done using organolithium compounds.

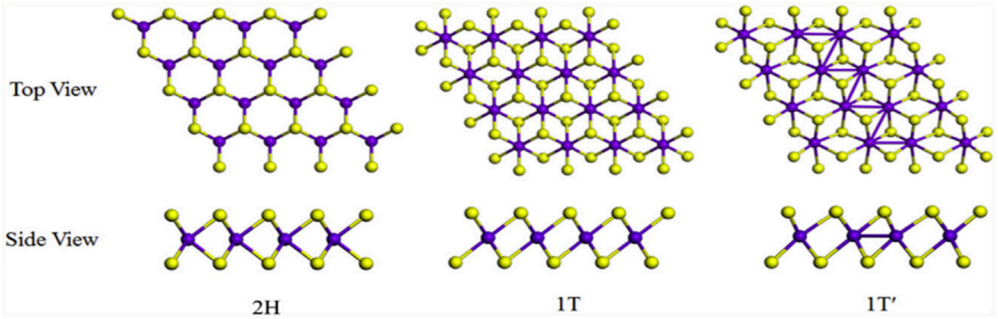

Figure 3. Top and side-view of MoS_2 monolayer crystalline phases [30]. Reprinted with permission from [30]. Copyright 2018. Elsevier.

Ball milling is also a top-down synthesis mechanism that is mostly used to obtain few-layered MoS_2 nanosheets. This approach is based on the process of milling, which reduces the size and layers of the compound, increasing its specific surface area. It was also used to prepare graphene layers from bulk graphite, which is a similar structure to that of MoS_2 [47]. The ball milling approach is also considered as a "green method", without requiring harmful chemicals, and can also be used as a simple and efficient method for obtaining qualitative MoS_2 nanosheets [48].

2.2. Bottom-Up Methods

Chemical vapor deposition (CVD) has always been a versatile bottom-up approach involved in obtaining large surface area MoS_2 on a substrate as a few-layered structure with great crystallinity. In CVD processes, a specific substrate is exposed to reactive precursors in a high pressure and temperature medium, in which they react or decompose to form high purity ultrathin films. Furthermore, via this method, the size and thickness of films can be controlled to obtain great crystal quality and desired electronic properties [49]. Some particular CVD techniques are sulfurization of Mo-based films and decomposition of molybdenum and sulfur-containing precursors [50,51]. The direct sulfurization of MoO_3 is one of the best ways to obtain great quality MoS_2. Using MoO_3 as a deposited surface on the substrate, it can react with sulfur precursors on its surface, generating the MoS_2 layers. The entire mechanism of CVD is explained by Hong et al. [52] Yongjie et al. [50] reported a direct preparation of single- and few-layered MoS_2 on SiO_2 substrates by pre-depositing Mo films followed by a CVD approach. They concluded that the size and thickness of MoS_2 films are dependent on the size of the substrate and the thickness of pre-deposited Mo, which are easily scalable and tuneable, making CVD an important approach for a large variety of applications.

Hydrothermal/solvothermal chemical synthesis is one of the most versatile approaches for obtaining MoS_2 structures, usually adopted for the preparation of molybdenum disulfide containing composites [33,50,51]. It is used to synthesize MoS_2 using Mo and S precursors via chemical reactions performed in high pressure of a tightly sealed autoclave placed in a medium temperature (i.e., <220 °C) [53,54]. During this synthesis, three steps take place: nucleation, aggregation and self-assembly of nanocrystals (Figure 4).

In this kind of process, precursors like MoO_3, sodium molybdate, ammonium heptamolybdate and sulfur precursors such as thiourea, thioacetamide, L-cysteine and sodium thiosulfate are dissolved in a solvent. The precursors are mixed together and are assisted by sonication, and then the synthesis is placed in a controlled medium at high pressure and temperature [55–57]. The obtained nanosheets will then aggregate and start to self-assemble to form microspheres and flower-like morphologies [58–60]. As a particular case, MoS_2/rGO composites were taken into account [33]. A scheme of MoS_2/rGO composite formation by this approach is presented in Figure 5.

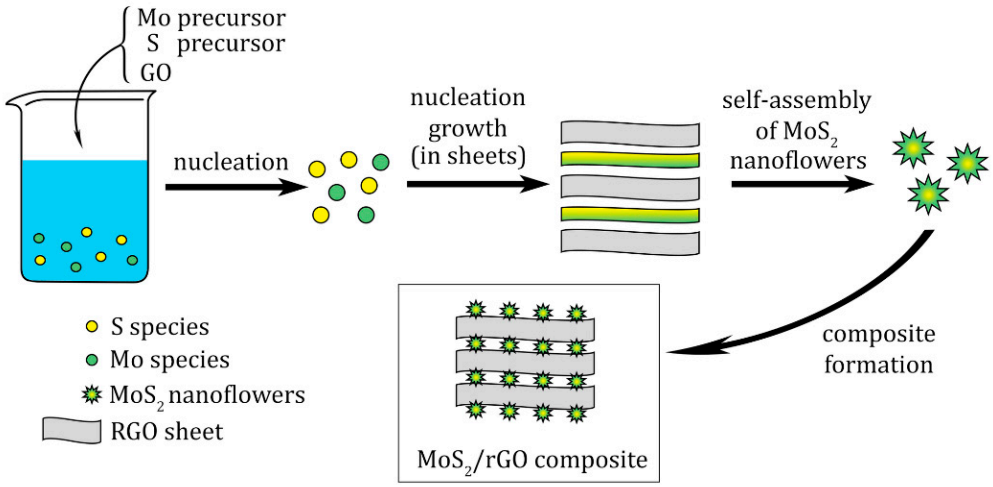

Figure 4. Formation of MoS_2/rGO composites following the three-step process of hydrothermal synthesis.

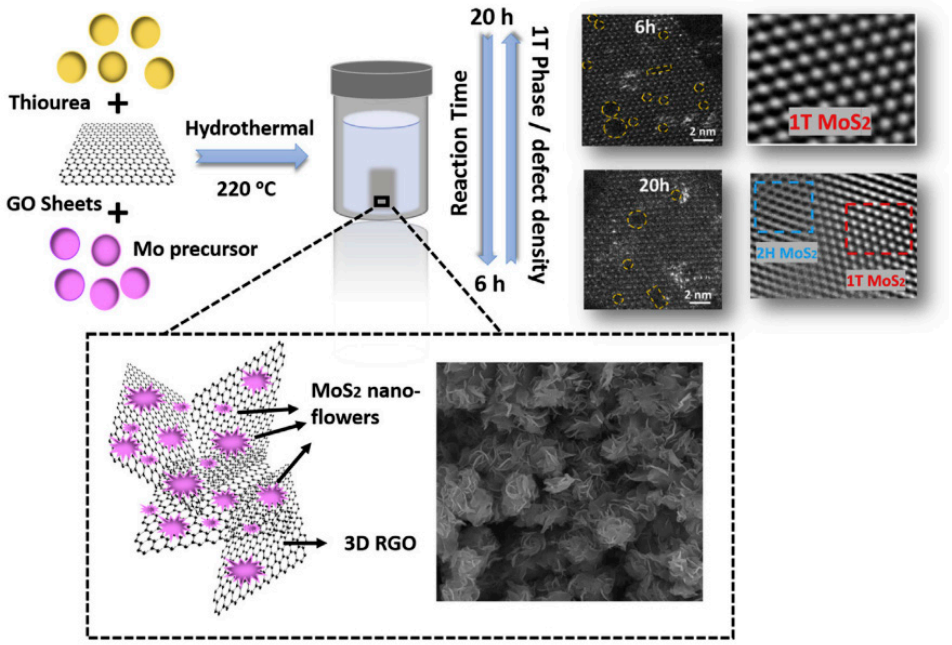

Figure 5. Scheme representing the formation of defective 1T MoS_2 nanoflowers on rGO substrate [37]. Reprinted with permission from [37]. Copyright 2019. Elsevier.

It is an approach based on a time-dependent evolution, starting with the nucleation phase, followed by nanosheet growth and aggregation, and the self-assembly of the nanosheets as a final step. Zheng et al. [36] carried out a series of time-dependent experiments in order to explore the formation mechanism of MoS_2 porous flower-like microspheres.

In more detail, the nucleation step starts firstly with the development of a nucleus and is subsequently continued by a growing stage, known as Ostwald ripening process [61]. This final process is a two-phase transformation of a thermodynamically unstable mixture. An increase in the size scale of a second phase and a decrease in the total interfacial area can reduce the system's energy. In other words, decreasing the system's energy by lowering the total surface area greatly influences the morphology of the product [61]. In the first step of a hydrothermal method, under controlled conditions, the molecules and ions gather around the nucleation area due to a concentration gradient and thermal convection. Usually, sulfur sources such as thioacetamide, thiourea and L-cysteine can easily coordinate with molybdate species because of the reductive -NH_2 functional group and combine with

the oxygen atoms of the molybdate species. Afterwards, the residual Mo and S, can bond into MoS_2 nuclei, which tend to aggregate into larger structures, minimizing the surface energy, in accordance with the Ostwald principle [36,62]. The second part of the formation mechanism consists of the aggregation of nuclei in nanosheets and the formation of petal-like layers on the surface of the larger particles [36]. Thus, the stacking process is uneven, due to the fact that in a layer structure the interlayer interactions and stress will be produced by local stacking. To reduce the internal stress and to minimize the surface energy over the structure, nanosheets will tend to bend [63]. Bending of the structure can also be seen in the grain boundaries of polycrystalline graphene [64]. Defects in the layered structure also affect the morphology of the composites. The two-phase hybridization of MoS_2 can also play an important role in this process because MoS_2 exhibits different electronic structures, such as a semiconducting ones (2H) and a metallic ones (1T). In other words, many processes, such as stacking, the existence of defects in the lattice and the presence of different phases of MoS_2 play key roles in the aggregation and bending growth of the composite.

The self-assembly process is dictated by the unstable structures of MoS_2, which tend to combine. The obtained hierarchical aggregated MoS_2 nanosheets have a high surface area. Baig et al. [65] had obtained flower-like structures with a specific surface area of 391 m^2g^{-1} for a MoS_2/rGO composite with ammonium hepta-molybdate and thiourea as precursors. Moreover, Chao et al. [31] reported specific surface areas of different MoS_2 composites such as 11.2 m^2g^{-1} for MoS_2/polyaniline (PANI), 31.4 m^2g^{-1} for MoS_2/rGO and 85.3 m^2g^{-1} for MoS_2/PANI/rGO. It was also reported that the size of nanosheet aggregates grows from 400 to 680 nm as the reaction period increases from 6 to 20 h [37], so they possess high surface energy. This is the primary reason for the MoS_2 nanosheets to make contact. As a result, they begin to expand and bend in order to decrease the surface energy and internal stress. The charge difference between the inner surface and the outer surface of the edges tends to lower or even disappear due to the effect of electron shielding [61]. At this stage, many connections will be formed between the surface and the edges of MoS_2 in order to minimize the specific surface area and energy, and the self-assembly process will continue until flower-like or sphere-like morphologies emerge, as was already reported [35,66–68].

3. The Influence of Preparation Parameters on Morphology, Structure and Surface Particularities of MoS_2/MoS_2-rGO Composites for Designing Efficient Supercapacitors

As pointed out above, there are some key preparation parameters and important processes that can influence the morphology, structure and surface particularities of MoS_2/MoS_2-rGO composites, such as reaction time, reducing agent, precursors, surfactants and molar ratios of molybdenum and sulphur sources. Further on, we will discuss the influence and interactions of these parameters from the perspective of the way they can affect the final properties. In order to understand the process as a whole mechanism, parameters and their contribution to this approach were taken into account.

3.1. Influence of the Reaction Time in MoS_2 and Its Composites Synthesis

Reaction time is definitely an important parameter in the synthesis of MoS_2 and its composites, especially when it comes down to hydrothermal technique, which affects the morphological, structural and surface area of the active material. Tang et al. [29] visualized by TEM technique the structural particularities of the formed MoS_2 after 6, 12 and 48 h of reaction time (Figure 6).

It was observed that with an increase in the reaction time to 48 h, a perfect crystalline flower-like MoS_2 structure was achieved. Based on the formation mechanism, which is time-dependent, it can be inferred that the sulfur sources are bound onto the surface of reduced graphene oxide via nucleation, forming MoS_2 nanoflowers that overlay both sides of the rGO. In terms of morphology, Naz et al. [37] reported an increase in nanosheet size from 400 to 680 nm, with a reaction time increase from 6 to 20 h at a temperature of 220 °C, respectively, and the formation of small nanoflowers with numerous edge sites. They also

reported that by increasing the reaction time, the thickness of MoS_2 nanosheets rises from 4.8 to 15 nm, and the number of layers from 6–7 to more than 15.

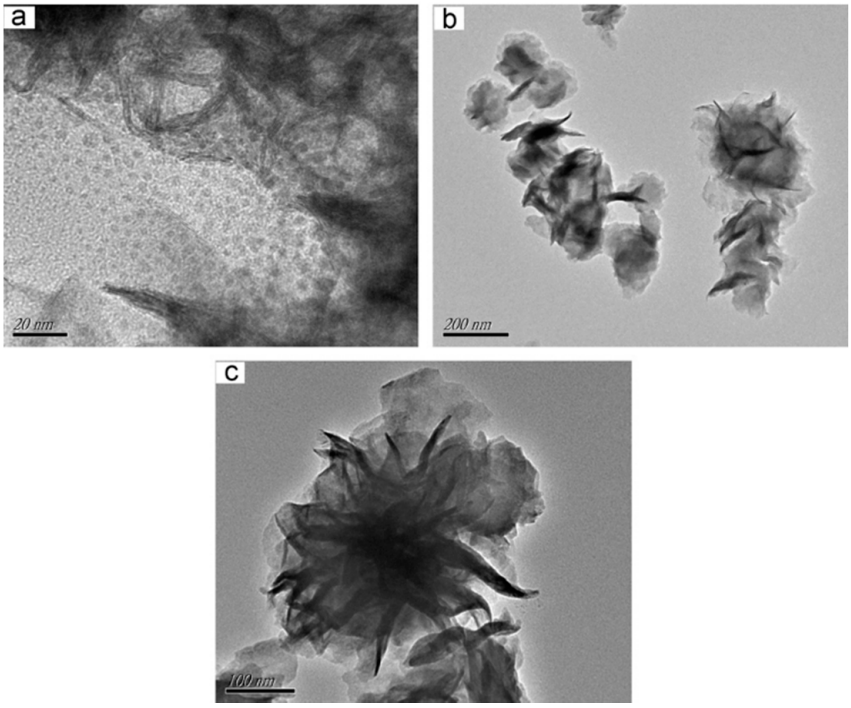

Figure 6. TEM images of MoS_2 samples obtained under different reaction times ((**a**): 6 h, (**b**): 12 h, (**c**): 48 h) from [29]. Reprinted with permission from [29]. Copyright 2012. Elsevier.

Zheng et al. [36] also performed a series of time-dependent experiments to explore the formation mechanism of MoS_2 flower-like microspheres, varying the synthesis reaction time (4, 8, 12, 16 and 22 h) and divided the whole mechanism into three phases, as discussed in the previous sections: nucleation, aggregation and self-assembly. It can be concluded that, in a hydrodynamic process, the formation of flower-like structures is time-dependent, meaning that a higher reaction time can deliver a more porous structure. However, other parameters, such as reducing agent and surfactants, which will be discussed later, must be taken into account to fully control the formed flower-like structures.

The specific surface area is also impacted by the reaction time as Manuraj et al. showed in their work [27]. They synthesised MoS_2 nanostructures using different reaction times (i.e., 12, 24, 36, 48 h) and proceeded, with BET analyses, the measurements of the surface area. They obtained the following results for the specified times: 10.74, 13.68, 18.45 and 13.26 m^2g^{-1} and pore diameters of 0.047421, 0.042381, 0.064782 and 0.035250 cm^3g^{-1}, respectively. These results showed that the maximum surface area and pore volume was exhibited at 36 h reaction time [27].

One should emphasize that which was reported by Naz et al. [37] relating to the presence of different defects in the composite lattice after 6 h of synthesis, after performing HAADF-STEM measurements. These defects consisted of the appearance of 3–5 nm holes, mainly due to varying quantities and shapes of atoms. They also concluded that the number of defects is higher in the sample synthesised after 6 h than those present into the 20 h synthesized one. They reported by Inductively Coupled Plasma Optical Spectroscopy (ICP-OS) analysis that the weight percentage of MoS_2 rises by 5.2% (from 56.6 to 61.8%) with the increase of the reaction time. Their XRD analysis showed a shift of the (002) peak from about $2\theta = 14^\circ$ to lower angles compared with that observed at $2\theta = 14.4^\circ$ for bulk 2H-MoS_2 phase, indicating a transition to the 1T phase. Moreover, another peak corresponding to (103) plane at $2\theta = 39.7^\circ$ confirmed the existence of a rich 2H phase as the reaction time was increased from 10 to 20 h [37].

In their work, Naz et al. [37] measured the XPS spectra of their composites synthesised with 6 h and 20 h of reaction time. The samples obtained after 6 h synthesis time show an Mo spectrum consisting of two major peaks at 228.7 and 231.8 eV, which correspond to $3d_{5/2}$ and $3d_{3/2}$ components, providing substantial evidence for the presence of 1T-phase of MoS_2. It was also calculated that the 1T-phase percentage was around 70–76%, while for the 2H-phase it was around 24–30%. The sample obtained with a 20 h reaction time had both peaks shifted towards higher bonding energy, at 229.4 eV for $3d_{5/2}$ and 232.5 eV for $3d_{3/2}$. Additionally, a broadening of the peaks was noticed, indicating the presence of a dominant 2H-phase at a percentage of about 60–63%. It was found in the fine spectrum of S that the signals at $2p_{3/2}$ and $2p_{1/2}$ shift to higher energy values with the increase of reaction time as follows: from 161.6 to 162.6 eV, and from 162.8 to 163.8 eV, respectively. The C 1 s components were also analysed by keeping in mind the evidence of GO deoxygenation (i.e., the reduction of GO) during hydrothermal process as the reaction time increases [37]. As it is known, GO contains many oxygen-containing functional groups like C=O, C-OH, O-C-O, HO-C=O etc., with broad peaks ranging from 280 to 290 eV [69]. Naz et al. [37] performed XPS measurements under the same conditions, but without GO substrate, and the sharp peaks recorded at 229.5 eV, for $3d_{5/2}$, and 232.5 eV, for $3d_{3/2}$, indicating the presence of pure 2H-phase of MoS_2. The obtained results demonstrated that the GO substrate has an important role in the growth and transition of 1T-phase MoS_2, which can be associated with the functional groups of GO.

3.2. The Influence of Surfactants for Synthesising MoS_2 and Its Composites

Usually, in the hydrothermal synthesis processes, the surfactant plays an essential role in controlling and altering the morphology of MoS_2 composites and preventing the restacking of MoS_2 and GO sheets [70]. Among the surfactants used, the followings stand out: cetyltrimethylammonium bromide (CTAB), sodium dodecyl sulfate (SDS), sodium dodecyl-benzene-sulfonate (SDBS), polyvinylpyrrolidone (PVP) or octyl phenol ethoxylate (Triton TX-100) [28,29,40].

Wu et al. [21] prepared MoS_2 hollow nanospheres using CTAB as a surfactant in a hydrothermal process. They claim that the amount of CTAB surfactant used increases the stacking of MoS_2 nanolayers, and that processing factors such as pH and CTAB surfactant can change the morphology. Nanosheets with a thickness of a few nanometers coil up and stretch towards the edge of hollow of flower-like microspheres and nanosheets according to their report. Since CTAB acts as a "soft" template for synthesising hollow nanomaterials, when the amount of CTAB surfactant is increased to 200 mg, well-defined hollow MoS_2 is formed [21].

Tang et al. [27] synthesised MoS_2 by the hydrothermal method, obtaining irregular nanosheets aggregated together to form flower-like structures of approximately 1–2 µm in size using about 180 mg of CTAB. They conducted a EDX analysis that revealed that the nanoflowers consisted of Mo and S elements. Moreover, the quantification of the peaks has shown an atom ratio of 1.98:1, which is very close to the stoichiometry of MoS_2 [29].

Hongtao et al. [40] synthesised MoS_2/rGO using the same procedure [27], but with three different surfactants such as CTAB, SDS and Triton X-100 to investigate their influence over composite's morphology. In the case of SDS, the GO flakes were compacted and the MoS_2 particles were scattered on them. Using Triton X-100 as surfactant they observed that the MoS_2 particles were wrapped by the paper-like rGO flakes. They reported that by using CTAB the MoS_2 particles were seen clearly and evenly distributed onto the rGO flakes and had a diameter of 1µm. They also reported that the three peaks (2θ = 14, 33.4, 58.9), which are indicative of the hexagonal MoS_2 phase, are sharper for the MoS_2/rGO-CTAB composite, indicating a higher crystallinity. In terms of specific surface area, they also reported that CTAB was the best candidate, the sample exhibiting a surface area of 133 m^2g^{-1}, while in the case of involving SDS and Triton X-100, the specific surface areas of 96 m^2g^{-1} and 27 m^2g^{-1} were achieved, respectively [40]. They performed XPS analysis on the CTAB-assisted sample, the recorded wide spectrum revealing the presence of C 1 s spectra at

285.1 eV, O 1s at around 533.2 eV, Mo 3d around 232.3 eV and S 2p at 163.1 eV. They divided the C 1s spectrum into three peaks corresponding to C=C bonds at 284.5 eV, C-O groups at 285.6 eV, and C=O bonds at 288.9 eV, which indicated the high deoxygenation of rGO. They also acquired the spectrum for Mo 3d and S 2p and highlighted the formation of crystalline MoS_2 [40].

Cui et al. [28] also reported a MoS_2 synthesis method using CTAB, SDBS and PVP, in which they pointed out the effects of surfactants on the morphology of MoS_2 using an SEM technique (Figure 7). It was shown that the bigger and most regular MoS_2 nanospheres were obtained by using CTAB as a surfactant. The positively charged CTAB attracts the negative charges of MoS_2, forming highly dispersed microspheres. However, the anionic surfactant SDBS presented negative charges in a water-based solution, resulting in poor MoS_2 dispersion. The macromolecular hydrophilic film of non-ionic surfactant PVP was formed on the surface of MoS_2 particles, early nucleation of MoS_2 was inhibited and agglomeration was avoided [28].

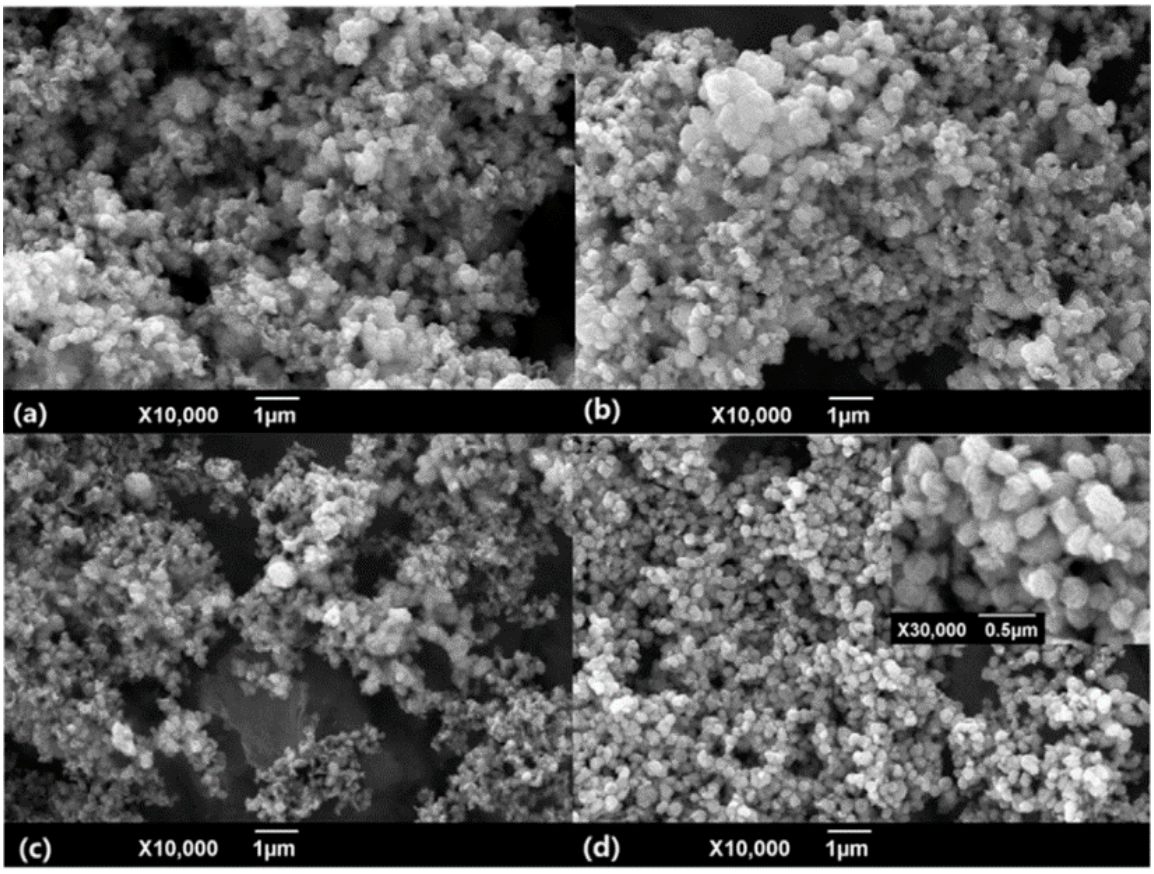

Figure 7. SEM images of MoS_2 microspheres prepared at 220 °C in pH 6 solution adding different surfactants (Mo/S ratio of 1:2): (**a**) no adding; (**b**) adding CTAB; (**c**) adding SDBS; (**d**) adding PVP [28]. Reprinted with permission from [28]. Copyright 2016. Elsevier.

3.3. The Influence of Reducing Agents for the Synthesis of MoS_2 and Its Composites

Another important parameter for the synthesis of MoS_2 and MoS_2 composites is the reducing agent, which can control the morphology. Zheng et al. [36] used different Mo and S precursors where the S precursor acts as a sulfur source and reducing agent and divided their combination into three groups. The first one, when $(NH_4)_6Mo_7O_{24}/H_2NCSNH_2$ and $Na_2MoO_4{\cdot}2H_2O/CH_3CSNH_2$ were used, a flower-like hollow microsphere was formed, while in the case of the second group, where a single compound in the obtaining for which $(NH_4)_6Mo_7O_{24}/Na_2S_2O_3{\cdot}5H_2O$ was used, morphology of a micron-sheet wrin-

kled surface was achieved, via a hydrothermal reaction. The third group, obtained using $Na_2MoO_4 \cdot 2H_2O$ and $(NH_4)_6Mo_7O_{24}$ and thioacetamide was made up of a blocky amorphous structure with particle sizes between 10 and 50 nm. The XRD patterns of the first group exhibited sharp peaks at $2\theta = 14°$, 33°, 38° and 58° that correspond to (002), (001), (103) and (100) lattice planes of the hexagonal structure of MoS_2, indicating a high crystallinity and a well-developed stacking. The second group's crystallinity was slightly decreased and the third one's were inconclusive, probably due to the amorphous structure [36].

Cui et al. [28] prepared MoS_2 microspheres through a surfactant-assisted hydrothermal synthesis using thioacetamide as the reducing agent. They deducted that compared to a thiourea containing system, the thioacetamide has a slower breakdown rate to form H_2S, which does contribute to the sulfuration of MoO_3 species. Ammonium heptamolybdate decomposition is also aided by the presence of H^+. However, the excess of H^+ increases the rate at which the thioacetamide decomposes to generate H_2S, potentially resulting in an inadequate reduction of MoO_3, lowering the purity and crystallinity of the synthesised MoS_2. It was also suggested that the electrostatic interactions might explain the modifying impact of surfactants, and that the effects of MoS_2 particles with a net negative charge on the surface was attracted by the positive charges of CTAB [28].

3.4. The Influence of the Molar Ratios of Molybdenum and Sulfur Precursors for Synthesising MoS_2 and Its Composites

Cui et al. [28] synthesised MoS_2 microspheres through a surfactant-assisted hydrothermal method using thioacetamide as a reducing agent. Their synthesis was done at 220 °C for different Mo to S ratios of 1:1, 1:2, 1:3, 1:4, and 1:5. They analysed the structure by X-ray diffraction. The sample with a Mo/S ratio of 1:2 exhibited a major diffraction peak that matched the 2H-phase two-layered hexagonal MoS_2. They stated that the recorded signals became broader with the decrease of Mo/S to 1:3, a result which indicated the presence of an amorphous structure. The same diffraction patterns as the one of 1:3 sample were observed in the other two samples with a Mo/S ratio of 1:4 and 1:5. XPS analyses of the MoS_2 samples prepared at 220 °C, at a pH of 6, without any surfactant, were also performed. The binding energy of 230.9 eV and 233.7 eV were found to correspond to the Mo $3d_{5/2}$, and Mo $3d_{3/2}$ orbitals of Mo(IV). The orbitals of S(II) were associated with S $2p_{3/2}$ and S $2p_{1/2}$ with the binding energy around 163.1 eV and 164.5 eV, respectively. By calculating the peak areas, the atom ratio of Mo to S was of about 1:2, which corresponds to MoS_2 and confirmed the previously reported results [28].

Sun et al. [71] synthesised 3D graphene/MoS_2 composites as electrode materials for supercapacitors and used GO, Na_2MoO_4 and thiourea as precursors. They prepared samples using different amounts of sodium molybdate and thiourea corresponding to mass ratio of MoS_2 to GO in composites of 1.1:1, 1.6:1, 2.1:1, 3.2:1, 4.2:1, and 5.3:1. For the first three samples, their SEM analysis showed MoS_2 nanosheets growing on the GO substrate. With the increase of Na_2MoO_4, for the next two samples they observed the formation of MoS_2 nanoflowers on the GO substrate and, ultimately the last sample with the highest Na_2MoO_4 concentration showed that the nanoflowers started to grow on top of the other MoS_2 nanoflowers instead growing on the GO substrate. Their results demonstrated that the morphology can change with the increase of Na_2MoO_4 content [71]. The 4:2:1 mass ratio sample's crystal phase and structure was compared to that of 3D GO, and MoS_2 through XRD analysis and concluded that their XRD patterns were quite similar, thus pointing out that GO has little effect on nucleation phase and growth of MoS_2. This observation highlights that 3D GO can be an appropriate platform for synthesising the composite, because graphene layers are dispersed and surrounded by MoS_2 layers [71]. BET surface analysis was used to determine the specific surface area, and the results for the first five samples were consistent with their morphologies, with an increase from 64.4 m^2g^{-1} to 165.7 m^2g^{-1} for samples with a mass ratios of 1.1:1 and 4.2:1, respectively [71].

Liu et al. [1] prepared MoS_2/rGO by hydrothermal method at 180 °C for 20 h using $(NH_4)Mo_7O_{24} \cdot 4H_2O$ and L-cysteine as precursors. They used different percentages of

MoS_2 to obtain composites, as follows: 35.8 wt%, 50.5 wt% and 60.8 wt%. The morphology and structure of MoS_2 show a highly porous structure enclosed by ultrathin sheets. The MoS_2 composite has nanosheets with a thickness of 1–3 layers uniformly dispersed on the rGO. By increasing the weight percentage of MoS_2, they obtained an increase in sheet thickness of 4–6, 7–9 and >10 for the simple MoS_2. The XRD patterns of rGO and MoS_2 can be assigned to the plane hexagonal structure of MoS_2 and the d_{002} plane of graphite. They stated that with the increase in the molybdenum disulfide concentration, the diffraction peaks of MoS_2 become higher in intensity, as expected, and the lattice spacing of the (002) plane of MoS_2 observed was 0.619. The group characterised the electronic structure of the composites by XPS analysis. The Mo 3d spectra showed dominant Mo^{4+} and traces of Mo^{6+} species corresponding to 2H-phase of MoS_2. The S 2p XPS spectra were also assigned to the 2H-phase. They observed that with the decrease in MoS_2 content, the intensities of Mo^{6+}-O and SO_x species rose gradually due to the increased proportion of the strong interaction between rGO and MoS_2 [1].

Peng et al. [41] reported a synthesis of MoS_2/rGO by hydrothermal method using $(NH_4)_6Mo_7O_{24}{\cdot}4H_2O$ and NH_2CSNH_2 at 200 °C for 24 h. The composites were prepared using 2:1 and 3:2 volume ratios of water and ethanol as solvents. The morphology of these composites revealed that the nanosheets of molybdenum disulfide were stacked and displayed in a 3D flower-like architecture. For the first sample with the volume ratio of 2:1, a porous flower-like morphology with corrugated and scrolled rGO sheets was obtained. With the decrease from 2:1 to 3:2 volume of water, the flower-like architecture vanished and changed to nanoflakes of MoS_2 on the surface of the rGO sheets. The XRD patterns showed peaks at $2\theta = 13.9°$, 33.4° and 59.1° attributed to (002), (100) and (110) planes of MoS_2 that indicated a successful load onto the rGO substrate. They calculated the corresponding d_{002} plane by the Bragg equation and found that it increased from 0.630 nm, for the blank, to 0.949 nm and 0.933 nm, for the 2:1 and 3:2 sample, respectively. The BET surface area was determined and the best results obtained were 28.7 m^2g^{-1}, 23.4 m^2g^{-1}, and 16.1 m^2g^{-1}, for the samples with the water to ethanol ratio of 2:1, 3:2, and the samples prepared in water as a solvent respectively. It was concluded that the solvent plays a substantial role and had an obvious effect on the surface structure of the resulting composites [41].

4. Electrical and Capacitive Properties for MoS_2-Based Electrode Materials in Energy Storage Applications

In this section, several promising results of electrode materials regarding the specific capacity and cycling stability will be presented. The results are also briefly presented in Table 1. We compiled a list of accomplishments based on key parameters, such as specific capacitance and cycling stability of electrode materials for supercapacitor applications, and ranked them in order of performance.

A different strategy to synthesize MoS_2 nanospheres was approached by Wang et al., [72] who used $MnCO_3$ as a template to grow the nanospheres and removed them afterwards by acid washing. Using $MnCO_3$, sodium molybdate and L-cysteine in a hydrothermal process, followed by acid washing to remove the template, they managed to obtain MoS_2 nanospheres with a specific capacity of 142 $F{\cdot}g^{-1}$ at a current density of 0.59 $A{\cdot}g^{-1}$ and a cycling stability of 92.9% after 1000 cycles [72].

Another electrode material synthesized by Liu et al. is MoS_2/GO [73]. After hydrothermal synthesis of molybdenum disulfide and its intercalation with N-buthyllithium, the GO was mixed with a poly(ethyleneimine) solution. Their material reported a specific capacitance of 153.9 $F{\cdot}g^{-1}$ at 5 $A{\cdot}g^{-1}$ with a cycling retention of 96% over 6800 cycles [73].

Table 1. Various results from literature on electrode materials based on MoS_2 composites for supercapacitor applications.

Composite	Precursors	Surfactant	Synthesis Method	Morphology	Synthesis Conditions	Specific Capacitance ($F \cdot g^{-1}$)	Specific Surface Area ($m^2 \cdot g^{-1}$)	Cycling Stability	Collectors	Electrode Test System	Electrolyte	References
C/MoS_2	Na_2MoO_4 and $C_3H_7NO_2S$	β-cyclodextrin	Hydrothermal	Flower-like	200 °C for 12 h	394 at 5 mV/s	6.36	60.68% after 2000 cycles at 40 mV/s	Stainless Steel	Three electrode system	1 M Na_2SO_4	[53]
MoS_2/rGO	$(NH_4)_6Mo_7O_{24}$ and CH_4N_2S	-	One pot reaction	Nanospheres	90 °C for 8 h	275 at 1 $A \cdot g^{-1}$	9.02	97% after 5000 cycles at 1 $A \cdot g^{-1}$	Ni foam	Two electrode system	6 M KOH	[75]
MoS_2/G	Na_2MoO_4 and CH_4N_2S	-	Hydrothermal	3D spheres	180 °C for 36 h	243 at 1 $A \cdot g^{-1}$	102.8	92.3% after 1000 cycles at 1 $A \cdot g^{-1}$	Stainless Steel	Three electrode system	1 M Na_2SO_4	[54]
MoS_2/rGO	$(NH_4)_6Mo_7O_{24}$ and C_2H_5NS	Citric Acid	Hydrothermal	Wrinkly paper like	180 °C for 24 h	334 at 0.5 mV/s	-	90% after 500 cycles at 10 mV/s	Platinum strip	Three electrode system	1 M $LiClO_4$	[33]
MoS_2/rGO	$(NH_4)_6Mo_7O_{24}$ and $C_3H_7NO_2S$	-	Hydrothermal	Wrinkly paper like	180 °C for 20 h	361 at 5 mV/s	-	92% after 10,000 cycles	Carbon paper	Two & Three electrode system	1 M H_2SO_4	[1]
MoS_2/Ni foam	Na_2MoO_4 and CH_4N_2S	CTAB	Hydrothermal	Hollow nanostructure	160–200 °C for 24 h	160.1 at 1 $A \cdot g^{-1}$	-	94.8% after 3000 cycles at 1 $A \cdot g^{-1}$	Ni foam	Three electrode system	1 M Na_2SO_4	[21]
MoS_2	Na_2MoO_4 and C_2H_5NS	-	Hydrothermal	Brush like	180 °C for 36 h	244 at 1 $A \cdot g^{-1}$	18.45	92% after 9000 cycles at 5 $A \cdot g^{-1}$	Ni foam	Three electrode system	1 M KOH	[27]
MoS_2/G	$(NH_4)_6Mo_7O_{24}$ and CH_4N_2S	-	One pot reaction	Nanosheet grains	50 °C for 6 h	756 at 0.5 $A \cdot g^{-1}$	-	88% after 10,000 cycles at 0.5 $A \cdot g^{-1}$	Stainless steel	Three electrode system	1 M KOH	[74]
MoS_2	Na_2MoO_4 and $C_3H_7NO_2S$	-	Hydrothermal	Nanospheres	220 °C for 24 h	142 at 0.59 $A \cdot g^{-1}$	-	92.9% after 1000 cycles at 0.59 $A \cdot g^{-1}$	Ni foam	Three electrode system	1 M KCl	[72]
MoS_2/PANI/rGO	$(NH_4)_6Mo_7O_{24}$ and CH_4N_2S	-	Hydrothermal	Flower-like	200 °C for 48 h	330.7 at 10 $A \cdot g^{-1}$	85.3	81.9 % after 40,000 cycles at 10 $A \cdot g^{-1}$	Graphite paper	Three electrode system	1 M H_2SO_4	[31]
MoS_2/rGO	$MoO_3 \cdot H_2O$ and C_2H_5NS	Urea	Hydrothermal	Flake-like	210 °C for 18 h	441 at 1 $A \cdot g^{-1}$	163.6	84.2% after 1000 cycles	ITO	Three electrode system	1 M Na_2SO_4	[76]
MoS_2/N-doped 3D Graphene	$(NH_4)_6Mo_7O_{24}$ and CH_4N_2S	-	Hydrothermal	Flower-like	200 °C for 24 h	301.2 at 0.2 $A \cdot g^{-1}$	-	82% after 1000 cycles at 1 $A \cdot g^{-1}$	Glassy carbon	Three electrode system	1 M Na_2SO_4	[77]
MoS_2/G aerogel	Li intercalation	-	Hydrothermal	3D porous network	180 °C for 12 h	268 at 0.5 $A \cdot g^{-1}$	149.3	93% after 1000 cycles	Ti foil	Three electrode system	1 M Na_2SO_4	[78]
MoS_2/CNT	MoO_3 and KSCN	SDBS	Hydrothermal	Flower-like	220 °C for 24 h	74.05 at 2 $A \cdot g^{-1}$	92.25	80.8% after 1000 cycles at 1 $A \cdot g^{-1}$	Ni foam	Three electrode system	1 M Na_2SO_4	[79]
MoS_2	$(NH_4)_6Mo_7O_{24}$ and CH_4N_2S	-	Hydrothermal	Flower-like	220 °C for 24 h	255.65 at 0.25 $A \cdot g^{-1}$	-	70%	Graphite foil	Two electrode system	3 M KOH	[80]
MoS_2/rGO	$(NH_4)_6Mo_7O_{24}$ and CH_4N_2S	PVP	Hydrothermal	Flower-like	180 °C for 16 h	850 at 1 $A \cdot g^{-1}$	391	95.33% after 10,000 cycles at 2 $A \cdot g^{-1}$	Ni foam	Three electrode system	1 M KCl	[65]
MoS_2/rGO	$(NH_4)_6Mo_7O_{24}$ and CH_4N_2S	-	Hydrothermal	Flower-like	220 °C for 6 h	442 at 1 $A \cdot g^{-1}$	29.27	90.3% after 1000 cycles at 5 $A \cdot g^{-1}$	Glassy carbon	Three electrode system	1 M H_2SO_4	[37]
MoS_2/3D-G	Na_2MoO_4 and CH_4N_2S	-	Hydrothermal	Nanoflowers	200 °C for 24 h	410 at 1 $A \cdot g^{-1}$	165.7	90.3% after 10,000 cycles at 2 $A \cdot g^{-1}$	Ni foam	Three electrode system	1 M Na_2SO_4	[71]
MoS_2/PANI	MoS_2 powder and aniline	-	In situ chemical process	Flower-like	12 h ice bath polymerization	575 at 1 $A \cdot g^{-1}$	-	>98% after 500 cycles at 1 $A \cdot g^{-1}$	Stainless steel	Three electrode system	1 M H_2SO_4	[81]
MoS_2/rGO	Na_2MoO_4 and C_2H_5NS	CTAB	Hydrothermal	Nanoparticles	180 °C for 12 h	1022 at 0.3 $A \cdot g^{-1}$	133	-	-	-	-	[40]
MoS_2	MoO_3 and C_2H_5NS	-	Hydrothermal	Nanoflowers	200 °C for 12 h	1120	54.7	96% after 2000 cycles at 10 $A \cdot g^{-1}$	Ni foam	Three electrode system	3 M KOH	[26]

Wu et al. [21] prepared MoS_2 as an electrode material for supercapacitors via a hydrothermal method, assisted with CTAB. The material's morphology varied between flower-like, nanosheets and hollow structures, and is influenced by the pH and CTAB concentration. Their best results were reported to be the ones of hollow structures of MoS_2, with a specific capacitance of 160 $F{\cdot}g^{-1}$ at a current density of 1 $A{\cdot}g^{-1}$ and a cycling stability of 94.8% after 3000 cycles [21].

Huang et al. [54] reported a layered MoS_2-graphene composite with a sheet-like structure obtained by hydrothermal synthesis at 200 °C for 24 h using sodium molybdate and thiourea as the main precursors and GO obtained by a modified Hummers method. The maximum specific capacitance of the composite was recorded to be 243 $F{\cdot}g^{-1}$ at a discharge current density of 1 $A{\cdot}g^{-1}$ and a cycling stability with only 7.7% loss after 1000 cycles [54].

Vikraman et al. [74] obtained a mixed-phase MoS_2 decorated rGO hybrid composite through a facile one-pot synthesis, using ammonium molybdate and thiourea as the main precursors and synthesized them on a hot plate at 90 °C for 8 h. Their hybrid material showed a symmetrical capacitance of 275 $F{\cdot}g^{-1}$ at a current density of 1 $A{\cdot}g^{-1}$ and a cycling stability of 97% over 5000 cycles.

Murugan et al. [33] obtained a two-dimensional composite with MoS_2 nanosheets anchored on graphene by an in-situ hydrothermal method. Their method consisted of using ammonium heptamolybdate and thioacetamide as precursors and citric acid as a surfactant, proceeding in a stainless-steel autoclave for 24 h at 435 k (161.85 °C). Their nanosheet structure was reported to exhibit a specific capacitance of 334 $F{\cdot}g^{-1}$ at a scan rate of 10 $mV{\cdot}s^{-1}$ and also a retention of 95% after 500 cycles.

In terms of symmetrical supercapacitors, Liu et al. [1] synthesized an electrode material able to obtain high specific capacitance of 361 $F{\cdot}g^{-1}$ at 5 $mV{\cdot}s^{-1}$ and a good cycle stability in 1 M H_2SO_4. The materials were obtained by a hydrothermal method using ammonium molybdate tetrahydrate and L-cysteine accompanied by GO obtained by a modified Hummers method. The morphology obtained was presented as a highly porous structure enclosed by ultrathin MoS_2 sheets uniformly distributed on the rGO substrate.

Gao et al. [53] synthesized, by a hydrothermal method, carbon-anchored MoS_2 nanosheets using sodium molybdate, L-cysteine and β-cyclodextrine as precursors in the process at 200 °C for 12 h. Among their samples, C/MoS_2—5.0% had the best electrical and capacitive performances. They reported that their material specific capacitance at a CV scan rate of 5 $mV{\cdot}s^{-1}$ was 394.2 $F{\cdot}g^{-1}$, and after increasing the scan rate at 200 $mV{\cdot}s^{-1}$, it remained at 249.6 $F{\cdot}g^{-1}$. It also presented a good cycling stability with a retention in capacity of 60.68% for 2000 cycles at a scan rate of 40 $mV{\cdot}s^{-1}$ [53].

Sun et al. [71] managed to synthesize a composite based on 3D GO and MoS_2 with a flower-like structure, which was able to increase the performances of the electrode material in a supercapacitive cell. As main precursors, sodium molybdate and thiourea were chosen with different concentrations. Their best results showed a specific capacitance of 410 $F{\cdot}g^{-1}$ at 1 $A{\cdot}g^{-1}$, current density and a cycle stability of 80.3% over a continuous 10,000 cycles at 2 $A{\cdot}g^{-1}$.

Naz et al. [37] reported a highly defective 1T-phased MoS_2 on 3D rGO composite with flower-like morphology using the hydrothermal route. They tested different synthesis times using, as precursors, ammonium molybdate and thiourea for MoS_2 at 220 °C. The rGO was prepared by the Hummers method. Their best results were at a synthesis time of 6 h, capable of giving an exceptional specific capacitance of 442.0 $F{\cdot}g^{-1}$ at a discharge current density of 1 $A{\cdot}g^{-1}$ and also being able to retain 90.3% of its capacitance after 1000 cycles at 5 $A{\cdot}g^{-1}$.

Huang et al. [81] synthesized a composite based on MoS_2/PANI by in situ chemical oxidative polymerization directed by molybdenum disulfide. Their material maximum specific capacitance was of about 575 $F{\cdot}g^{-1}$ at 1 $A{\cdot}g^{-1}$ and a retention of less than 2% after 500 cycles at the same current density.

Dutta et al. [6] prepared a hybrid electrode material of MoS_2/rGO nanosheets by a hydrothermal route using SDS as a surfactant and MoO_3 and potassium thiocyanate as the main precursors, keeping them in a stainless steel autoclave at 220 °C for 24 h. Their results showed a specific capacitance of approximately $F \cdot g^{-1}$ and a retention of 95% after 1000 cycles using 1 M H_2SO_4 as electrolyte, with measurements being made in a three-electrode system.

Baig et al. [65] reported a composite material made of MoS_2/rGO with a specific capacitance of 850 $F \cdot g^{-1}$ at a current density of 1 $A \cdot g^{-1}$ and a cycle stability at 2 $A \cdot g^{-1}$ of 95.3% for over 10,000 cycles. To obtain the electrode material they used a hydrothermal method with ammonium heptamolybdate and thiourea as precursors and PVP as a main surfactant.

Hongtao et al. [40] tested different surfactants and their effect on the morphologies and electrical properties of a composite based on MoS_2/rGO. In their hydrothermal synthesis, they used sodium molybdate and thioacetamide as precursors for MoS_2 and a modified Hummers method for the rGO. They obtained different morphologies and properties based on the surfactant. However, the best results were given by using CTAB with the highest specific capacitance of 1022 $F \cdot g^{-1}$ at a current density of 0.3 $A \cdot g^{-1}$.

Self-assembled nanoflowers of MoS_2 were obtained by Wei et al. [26] Their method was based on a one-pot hydrothermal reaction from which they obtained flower-like MoS_2 capable of exhibiting 1120 $F \cdot g^{-1}$ at a current density of 0.5 $A \cdot g^{-1}$ in KOH electrolyte. Their cycling stability was measured at 10 $A \cdot g^{-1}$ current density and it showed a 96% retention in 2000 cycles.

5. Conclusions

A general conclusion might be that in developing more efficient electrode materials for supercapacitors, combining a conductive polymer like polyaniline (PANI) with a promising material like MoS_2 to obtain loose and porous structures with pseudocapacitive behaviour is a must. Using conductive materials such as rGO to create a structure to intercalate porous MoS_2 morphologies is also a good way to improve the electrode material's electrochemical properties and to develop better active materials. The key in developing better electrode materials for supercapacitor applications appears to be engineering the phase structure of MoS_2, as well as modelling its morphology and using the appropriate electrolyte.

To put it another way, better results can be obtained by selecting and engineering the appropriate materials for the development of efficient and long-lasting supercapacitors. Graphene, GO, and rGO, as well as conductive polymers like polyaniline, in combination with the porous, well-engineered phase MoS_2, could be a promising path forward in the energy storage field. Although, in order to achieve better materials and results, the synthesis route and parameters such as precursors, reaction time, surfactants used and molar ratios must be carefully considered.

Author Contributions: Conceptualization, C.A.S., L.C.C. and L.B.; writing—original draft preparation, C.A.S.; writing—review and editing, C.C. and L.C.C.; visualization, L.B. and L.C.C.; supervision, L.B. All authors have read and agreed to the published version of the manuscript.

Funding: This research was funded by UBB-TeMATIC-Art P_40_374 project.

Data Availability Statement: Not applicable.

Acknowledgments: C.C. acknowledges financial support from a special grant for scientific activity awarded by STAR-UBB (Babeş-Bolyai University).

Conflicts of Interest: The authors declare no conflict of interest.

References

1. Liu, Q.; Zhu, H.; Ma, Q.; Liu, M.; Wang, B.; Tang, C.; Wang, Y.; Wu, Q.; Wang, X.; Hu, Z. Ultrathin MoS_2 nanosheets hybridizing with reduced graphene oxide for high-performance pseudocapacitors. *FlatChem* **2020**, *26*, 100212. [CrossRef]
2. Liu, C.; Li, F.; Lai-Peng, M.; Cheng, H.M. Advanced materials for energy storage. *Adv. Mater.* **2010**, *22*, 28–62. [CrossRef]

3. Zhang, S.; Pan, N. Supercapacitors performance evaluation. *Adv. Energy Mater.* **2015**, *5*, 1401401. [CrossRef]
4. Salanne, M.; Rotenberg, B.; Naoi, K.; Kaneko, K.; Taberna, P.L.; Grey, C.P.; Dunn, B.; Simon, P. Efficient storage mechanisms for building better supercapacitors. *Nat. Energy* **2016**, *1*, 16070. [CrossRef]
5. Sarmah, D.; Kumar, A. Symmetric Supercapacitors with layer-by-layer Molybdenum disulfide—reduced graphene oxide structures and poly(3,4-ethylenedioxythiophene) nanoparticles nanohybrid electrode. *J. Energy Storage* **2021**, *35*, 102289. [CrossRef]
6. Dutta, S.; De, S. MoS_2 Nanosheet/rGO Hybrid: An Electrode Material for High Performance Thin Film Supercapacitor. *Mater. Today Proc.* **2018**, *5*, 9771–9775. [CrossRef]
7. Fan, X.; Xu, P.; Zhou, D.; Sun, Y.; Li, Y.C.; Nguyen, M.A.T.; Terrones, M.; Mallouk, T.E. Fast and Efficient Preparation of Exfoliated 2H MoS_2 Nanosheets by Sonication-Assisted Lithium Intercalation and Infrared Laser-Induced 1T to 2H Phase Reversion. *Nano Lett.* **2015**, *15*, 5956–5960. [CrossRef] [PubMed]
8. Pandolfo, A.G.; Hollenkamp, A.F. Carbon properties and their role in supercapacitors. *J. Power Sources* **2006**, *157*, 11–27. [CrossRef]
9. Frackowiak, E. Carbon materials for supercapacitor application. *Phys. Chem. Chem. Phys.* **2007**, *9*, 1774–1785. [CrossRef]
10. Béguin, F.; Presser, V.; Balducci, A.; Frackowiak, E. Carbons and electrolytes for advanced supercapacitors. *Adv. Mater.* **2014**, *26*, 2219–2251. [CrossRef]
11. Obreja, V.V.N. On the performance of supercapacitors with electrodes based on carbon nanotubes and carbon activated material—A review. *Phys. E Low-Dimens. Syst. Nanostructures* **2008**, *40*, 2596–2605. [CrossRef]
12. Gul, H.; Shah, A.-u.-H.A.; Bilal, S. Achieving ultrahigh cycling stability and extended potential window for supercapacitors through asymmetric combination of conductive polymer nanocomposite and activated carbon. *Polymers* **2019**, *11*, 1678. [CrossRef] [PubMed]
13. Vighnesha, K.M.; Shruthi; Sandhya; Sangeetha, D.N.; Selvakumar, M. Synthesis and characterization of activated carbon/conducting polymer composite electrode for supercapacitor applications. *J. Mater. Sci. Mater. Electron.* **2018**, *29*, 914–921. [CrossRef]
14. Hulicova-Jurcakova, D.; Seredych, M.; Lu, G.Q.; Bandosz, T.J. Combined effect of nitrogen- and oxygen-containing functional groups of microporous activated carbon on its electrochemical performance in supercapacitors. *Adv. Funct. Mater.* **2009**, *19*, 438–447. [CrossRef]
15. Cericola, D.; Ruch, P.W.; Kötz, R.; Novák, P.; Wokaun, A. Characterization of bi-material electrodes for electrochemical hybrid energy storage devices. *Electrochem. Commun.* **2010**, *12*, 812–815. [CrossRef]
16. Wang, Y.G.; Xia, Y.Y. A new concept hybrid electrochemical surpercapacitor: Carbon/$LiMn_2O_4$ aqueous system. *Electrochem. Commun.* **2005**, *7*, 1138–1142. [CrossRef]
17. Fan, Z.; Yan, J.; Wei, T.; Zhi, L.; Ning, G.; Li, T.; Wei, F. Asymmetric supercapacitors based on graphene/MnO2 and activated carbon nanofiber electrodes with high power and energy density. *Adv. Funct. Mater.* **2011**, *21*, 2366–2375. [CrossRef]
18. Yang, Z.M.; Vinodh, R.; Balakrishnan, B.; Rajmohan, R.; Kim, H.J. Rational design of asymmetric aqueous supercapacitor based on NAXMnO_2 and N-doped reduced graphene oxide. *J. Energy Storage* **2020**, *28*, 101293. [CrossRef]
19. Chen, B.; Lu, H.; Zhao, N.; Shi, C.; Liu, E.; He, C.; Ma, L. Facile synthesis and electrochemical properties of continuous porous spheres assembled from defect-rich, interlayer-expanded, and few-layered MoS_2/C nanosheets for reversible lithium storage. *J. Power Sources* **2018**, *387*, 16–23. [CrossRef]
20. Ke, Q.; Wang, J. Graphene-based materials for supercapacitor electrodes—A review. *J. Mater.* **2016**, *2*, 37–54. [CrossRef]
21. Wu, D.; Zhang, C.; Xu, S.; Zhu, Y.; Xiong, D.; Wang, L.; Chu, P.K. Fabrication and enhanced supercapacitance of hollow nanostructured MoS_2 prepared by a CATB-assisted hydrothermal process. *Mater. Lett.* **2016**, *184*, 96–99. [CrossRef]
22. Zhang, L.L.; Zhou, R.; Zhao, X.S. Graphene-based materials as supercapacitor electrodes. *J. Mater. Chem.* **2010**, *20*, 5983–5992. [CrossRef]
23. Yun, Q.; Li, L.; Hu, Z.; Lu, Q.; Chen, B.; Zhang, H. Layered Transition Metal Dichalcogenide-Based Nanomaterials for Electrochemical Energy Storage. *Adv. Mater.* **2019**, *32*, 1903826. [CrossRef]
24. Wang, H.; Feng, H.; Li, J. Graphene and Graphene-like Layered Transition Metal Dichalcogenides in Energy Conversion and Storage. *Adv. Mater.* **2014**, *10*, 2165–2181. [CrossRef]
25. Gao, M.R.; Xu, Y.F.; Jiang, J.; Yu, S.H. Nanostructured metal chalcogenides: Synthesis, modification, and applications in energy conversion and storage devices. *Chem. Soc. Rev.* **2013**, *42*, 2986–3017. [CrossRef]
26. Wei, S.; Zhou, R.; Wang, G. Enhanced Electrochemical Performance of Self-Assembled Nanoflowers of MoS_2 Nanosheets as Supercapacitor Electrode Materials. *ACS Omega* **2019**, *4*, 15780–15788. [CrossRef]
27. Manuraj, M.; Kavya Nair, K.V.; Unni, K.N.N.; Rakhi, R.B. High performance supercapacitors based on MoS_2 nanostructures with near commercial mass loading. *J. Alloys Compd.* **2020**, *819*, 152963. [CrossRef]
28. Cui, Y.; He, J.; Yuan, F.; Xue, J.; Li, X.; Wang, J. Preparation of MoS_2 microspheres through surfactants-assisted hydrothermal synthesis using thioacetamide as reducing agent. *Hydrometallurgy* **2016**, *164*, 184–188. [CrossRef]
29. Tang, G.; Sun, J.; Wei, C.; Wu, K.; Ji, X.; Liu, S.; Tang, H.; Li, C. Synthesis and characterization of flowerlike MoS 2 nanostructures through CTAB-assisted hydrothermal process. *Mater. Lett.* **2012**, *86*, 9–12. [CrossRef]
30. Jayabal, S.; Wu, J.; Chen, J.; Geng, D.; Meng, X. Metallic 1T-MoS_2 nanosheets and their composite materials: Preparation, properties and emerging applications. *Mater. Today Energy* **2018**, *10*, 264–279. [CrossRef]
31. Chao, J.; Yang, L.; Liu, J.; Hu, R.; Zhu, M. Sandwiched MoS_2/polyaniline nanosheets array vertically aligned on reduced graphene oxide for high performance supercapacitors. *Electrochim. Acta* **2018**, *270*, 387–394. [CrossRef]

32. Wang, X.; Ding, W.; Li, H.; Li, H.; Zhu, S.; Zhu, X.; Dai, J.; Sheng, Z.; Wang, H.; Zhu, X.; et al. Unveiling highly ambient-stable multilayered 1T-MoS_2 towards all-solid-state flexible supercapacitors. *J. Mater. Chem. A* **2019**, *7*, 19152–19160. [CrossRef]
33. Murugan, M.; Mohan Kumar, R.; Alsalme, A.; Alghamdi, A.; Jayavel, R. Synthesis and property studies of molybdenum disulfide modified reduced graphene oxide (MoS_2-rGO) Nanocomposites for Supercapacitor Applications. *J. Nanosci. Nanotechnol.* **2017**, *17*, 5469–5474. [CrossRef]
34. Shi, S.; Sun, Z.; Hu, Y.H. Synthesis, stabilization and applications of 2-dimensional 1T metallic MoS_2. *J. Mater. Chem. A* **2018**, *6*, 23932–23977. [CrossRef]
35. Bello, I.T.; Oladipo, A.O.; Adedokun, O.; Dhlamini, S.M. Recent advances on the preparation and electrochemical analysis of MoS_2-based materials for supercapacitor applications: A mini-review. *Mater. Today Commun.* **2020**, *25*, 101664. [CrossRef]
36. Zheng, X.; Zhu, Y.; Sun, Y.; Jiao, Q. Hydrothermal synthesis of MoS_2 with different morphology and its performance in thermal battery. *J. Power Sources* **2018**, *395*, 318–327. [CrossRef]
37. Naz, R.; Imtiaz, M.; Liu, Q.; Yao, L.; Abbas, W.; Li, T.; Zada, I.; Yuan, Y.; Chen, W.; Gu, J. Highly defective 1T-MoS_2 nanosheets on 3D reduced graphene oxide networks for supercapacitors. *Carbon N. Y.* **2019**, *152*, 697–703. [CrossRef]
38. Kumar, N.A.; Dar, M.A.; Gul, R.; Baek, J.B. Graphene and molybdenum disulfide hybrids: Synthesis and applications. *Mater. Today* **2015**, *18*, 286–298. [CrossRef]
39. Ma, L.; Ye, J.; Chen, W.; Wang, J.; Liu, R.; Lee, J.Y. Synthesis of Few-Layer MoS_2-Graphene Composites with Superior Electrochemical Lithium-Storage Performance by an Ionic-Liquid-Mediated Hydrothermal Route. *ChemElectroChem* **2015**, *2*, 538–546. [CrossRef]
40. Hongtao, L.; Zichen, X.; Lina, Z.; Zhiqiang, Z.; Li, X. The effects of different surfactants on the morphologies and electrochemical properties of MoS_2/reduce graphene oxide composites. *Chem. Phys. Lett.* **2019**, *716*, 6–10. [CrossRef]
41. Peng, W.; Wang, W.; Han, G.; Huang, Y.; Zhang, Y. Fabrication of 3D flower-like MoS_2/graphene composite as high-performance electrode for capacitive deionization. *Desalination* **2020**, *473*, 114191. [CrossRef]
42. Smith, R.J.; King, P.J.; Lotya, M.; Wirtz, C.; Khan, U.; De, S.; O'Neill, A.; Duesberg, G.S.; Grunlan, J.C.; Moriarty, G.; et al. Large-scale exfoliation of inorganic layered compounds in aqueous surfactant solutions. *Adv. Mater.* **2011**, *23*, 3944–3948. [CrossRef]
43. Sun, Y.; Gao, S.; Lei, F.; Xie, Y. Atomically-thin two-dimensional sheets for understanding active sites in catalysis. *Chem. Soc. Rev.* **2015**, *44*, 623–636. [CrossRef]
44. Acerce, M.; Voiry, D.; Chhowalla, M. Metallic 1T phase MoS_2 nanosheets as supercapacitor electrode materials. *Nat. Nanotechnol.* **2015**, *10*, 313–318. [CrossRef]
45. Vaia, R.A.; Ishii, H.; Giannelis, E.P. Synthesis and Properties of Two-Dimensional Nanostructures by Direct Intercalation of Polymer Melts in Layered Silicates. *Chem. Mater.* **1993**, *5*, 1694–1696. [CrossRef]
46. Bang, G.S.; Nam, K.W.; Kim, J.Y.; Shin, J.; Choi, J.W.; Choi, S.Y. Effective liquid-phase exfoliation and sodium ion battery application of MoS_2 nanosheets. *ACS Appl. Mater. Interfaces* **2014**, *6*, 7084–7089. [CrossRef]
47. Li, J.; Gao, D.; Wang, J.; Miao, S.; Wang, G.; Bao, X. Ball-milling MoS_2/carbon black hybrid material for catalyzing hydrogen evolution reaction in acidic medium. *J. Energy Chem.* **2015**, *24*, 608–613. [CrossRef]
48. Wang, H.; Tran, D.; Moussa, M.; Stanley, N.; Tung, T.T.; Yu, L.; Yap, P.L.; Ding, F.; Qian, J.; Losic, D. Improved preparation of MoS_2/graphene composites and their inks for supercapacitors applications. *Mater. Sci. Eng. B Solid-State Mater. Adv. Technol.* **2020**, *262*, 114700. [CrossRef]
49. Zhang, H. Ultrathin Two-Dimensional Nanomaterials. *ACS Nano* **2015**, *9*, 9451–9469. [CrossRef]
50. Zhan, Y.; Liu, Z.; Najmaei, S.; Ajayan, P.M.; Lou, J. Large-area vapor-phase growth and characterization of MoS_2 atomic layers on a SiO_2 substrate. *Small* **2012**, *8*, 966–971. [CrossRef] [PubMed]
51. Voiry, D.; Goswami, A.; Kappera, R.; Silva, C.D.C.C.E.; Kaplan, D.; Fujita, T.; Chen, M.; Asefa, T.; Chhowalla, M. Covalent functionalization of monolayered transition metal dichalcogenides by phase engineering. *Nat. Chem.* **2015**, *7*, 45–49. [CrossRef] [PubMed]
52. Hong, S.; Sheng, C.; Krishnamoorthy, A.; Rajak, P.; Tiwari, S.; Nomura, K.I.; Misawa, M.; Shimojo, F.; Kalia, R.K.; Nakano, A.; et al. Chemical Vapor Deposition Synthesis of MoS_2 Layers from the Direct Sulfidation of MoO_3 Surfaces Using Reactive Molecular Dynamics Simulations. *J. Phys. Chem. C* **2018**, *122*, 7494–7503. [CrossRef]
53. Gao, A.; Zeng, D.; Liu, Q.; Yi, F.; Shu, D.; Cheng, H.; Zhou, X.; Li, S.; Zhang, F. Molecular self-assembly assisted synthesis of carbon nanoparticle-anchored MoS_2 nanosheets for high-performance supercapacitors. *Electrochim. Acta* **2019**, *295*, 187–194. [CrossRef]
54. Huang, K.J.; Wang, L.; Liu, Y.J.; Liu, Y.M.; Wang, H.B.; Gan, T.; Wang, L.L. Layered MoS_2-graphene composites for supercapacitor applications with enhanced capacitive performance. *Int. J. Hydrog. Energy* **2013**, *38*, 14027–14034. [CrossRef]
55. Wang, M.; Li, G.; Xu, H.; Qian, Y.; Yang, J. Enhanced lithium storage performances of hierarchical hollow MoS_2 nanoparticles assembled from nanosheets. *ACS Appl. Mater. Interfaces* **2013**, *5*, 1003–1008. [CrossRef] [PubMed]
56. Wang, P.P.; Sun, H.; Ji, Y.; Li, W.; Wang, X. Three-dimensional assembly of single-layered Mos_2. *Adv. Mater.* **2014**, *26*, 964–969. [CrossRef]
57. Zhao, B.; Wang, Z.; Gao, Y.; Chen, L.; Lu, M.; Jiao, Z.; Jiang, Y.; Ding, Y.; Cheng, L. Hydrothermal synthesis of layer-controlled MoS_2 /graphene composite aerogels for lithium-ion battery anode materials. *Appl. Surf. Sci.* **2016**, *390*, 209–215. [CrossRef]

58. Fan, L.Q.; Liu, G.J.; Zhang, C.Y.; Wu, J.H.; Wei, Y.L. Facile one-step hydrothermal preparation of molybdenum disulfide/carbon composite for use in supercapacitor. *Int. J. Hydrog. Energy* **2015**, *40*, 10150–10157. [CrossRef]
59. Ma, L.; Chen, W.X.; Li, H.; Zheng, Y.F.; Xu, Z. De Ionic liquid-assisted hydrothermal synthesis of MoS_2 microspheres. *Mater. Lett.* **2008**, *62*, 797–799. [CrossRef]
60. Nagaraju, G.; Tharamani, C.N.; Chandrappa, G.T.; Livage, J. Hydrothermal synthesis of amorphous MoS 2 nanofiber bundles via acidification of ammonium heptamolybdate tetrahydrate. *Nanoscale Res. Lett.* **2007**, *2*, 461–468. [CrossRef]
61. Voorhees, P.W. The theory of Ostwald ripening. *J. Stat. Phys.* **1985**, *38*, 231–252. [CrossRef]
62. Xing, J.C.; Zhu, Y.L.; Zhou, Q.W.; Di Zheng, X.; Jiao, Q.J. Fabrication and shape evolution of CoS2 octahedrons for application in supercapacitors. *Electrochim. Acta* **2014**, *136*, 550–556. [CrossRef]
63. Zhang, K.; Hu, S.; Zhang, Y.; Zhang, T.; Zhou, X.; Sun, Y.; Li, T.X.; Fan, H.J.; Shen, G.; Chen, X.; et al. Self-induced uniaxial strain in MoS_2 monolayers with local van der waals-stacked interlayer interactions. *ACS Nano* **2015**, *9*, 2704–2710. [CrossRef] [PubMed]
64. Guo, X.; Yang, G.; Zhang, J.; Xu, X. Structural, mechanical and electronic properties of in-plane 1T/2H phase interface of MoS_2 heterostructures. *AIP Adv.* **2015**, *5*, 097174. [CrossRef]
65. Baig, M.M.; Pervaiz, E.; Yang, M.; Gul, I.H. High-Performance Supercapacitor Electrode Obtained by Directly Bonding 2D Materials: Hierarchal MoS_2 on Reduced Graphene Oxide. *Front. Mater.* **2020**, *7*, 580424. [CrossRef]
66. Nadeem Riaz, K.; Yousaf, N.; Bilal Tahir, M.; Israr, Z.; Iqbal, T. Facile hydrothermal synthesis of 3D flower-like La-MoS_2 nanostructure for photocatalytic hydrogen energy production. *Int. J. Energy Res.* **2019**, *43*, 491–499. [CrossRef]
67. Krishnamoorthy, K.; Veerapandian, M.; Yun, K.; Kim, S.J. The chemical and structural analysis of graphene oxide with different degrees of oxidation. *Carbon N. Y.* **2013**, *53*, 38–49. [CrossRef]
68. Ma, L.; Xu, L.M.; Zhou, X.P.; Xu, X.Y. Biopolymer-assisted hydrothermal synthesis of flower-like MoS_2 microspheres and their supercapacitive properties. *Mater. Lett.* **2014**, *132*, 291–294. [CrossRef]
69. Thangappan, R.; Kalaiselvam, S.; Elayaperumal, A.; Jayavel, R.; Arivanandhan, M.; Karthikeyan, R.; Hayakawa, Y. Graphene decorated with MoS_2 nanosheets: A synergetic energy storage composite electrode for supercapacitor applications. *Dalt. Trans.* **2016**, *45*, 2637–2646. [CrossRef]
70. Wang, Z.; Chen, T.; Chen, W.; Chang, K.; Ma, L.; Huang, G.; Chen, D.; Lee, J.Y. CTAB-assisted synthesis of single-layer MoS_2-graphene composites as anode materials of Li-ion batteries. *J. Mater. Chem. A* **2013**, *1*, 2202–2210. [CrossRef]
71. Sun, T.; Li, Z.; Liu, X.; Ma, L.; Wang, J.; Yang, S. Facile construction of 3D graphene/MoS_2 composites as advanced electrode materials for supercapacitors. *J. Power Sources* **2016**, *331*, 180–188. [CrossRef]
72. Wang, L.; Ma, Y.; Yang, M.; Qi, Y. Hierarchical hollow MoS_2 nanospheres with enhanced electrochemical properties used as an Electrode in Supercapacitor. *Electrochim. Acta* **2015**, *186*, 391–396. [CrossRef]
73. Liu, M.C.; Xu, Y.; Hu, Y.X.; Yang, Q.Q.; Kong, L.B.; Liu, W.W.; Niu, W.J.; Chueh, Y.L. Electrostatically Charged MoS 2 /Graphene Oxide Hybrid Composites for Excellent Electrochemical Energy Storage Devices. *ACS Appl. Mater. Interfaces* **2018**, *10*, 35571–35579. [CrossRef] [PubMed]
74. Vikraman, D.; Karuppasamy, K.; Hussain, S.; Kathalingam, A.; Sanmugam, A.; Jung, J.; Kim, H.S. One-pot facile methodology to synthesize MoS_2-graphene hybrid nanocomposites for supercapacitors with improved electrochemical capacitance. *Compos. Part B Eng.* **2019**, *161*, 555–563. [CrossRef]
75. Vikraman, D.; Rabani, I.; Hussain, S.; Sundaram, K.; Ramesh, S.; Kim, H.S.; Seo, Y.S.; Jung, J.; Kim, H.S. Mixed-phase MoS_2 decorated reduced graphene oxide hybrid composites for efficient symmetric supercapacitors. *Int. J. Energy Res.* **2021**, *45*, 9193–9209. [CrossRef]
76. Sabeeh, H.; Zulfiqar, S.; Aadil, M.; Shahid, M.; Shakir, I.; Khan, M.A.; Warsi, M.F. Flake-like MoS_2 nano-architecture and its nanocomposite with reduced Graphene Oxide for hybrid supercapacitors applications. *Ceram. Int.* **2020**, *46*, 21064–21072. [CrossRef]
77. Liu, Z.; Qin, A.; Yang, B.; Wang, D.; Zhang, Z. Flower-like MoS 2 onto nitrogen-doped 3D graphene composite with active material for supercapacitor electrodes. *Mater. Lett.* **2019**, *240*, 258–261. [CrossRef]
78. Yang, M.H.; Jeong, J.M.; Huh, Y.S.; Choi, B.G. High-performance supercapacitor based on three-dimensional MoS_2/graphene aerogel composites. *Compos. Sci. Technol.* **2015**, *121*, 123–128. [CrossRef]
79. Chen, M.; Dai, Y.; Wang, J.; Wang, Q.; Wang, Y.; Cheng, X.; Yan, X. Smart combination of three-dimensional-flower-like MoS_2nanospheres/interconnected carbon nanotubes for application in supercapacitor with enhanced electrochemical performance. *J. Alloys Compd.* **2017**, *696*, 900–906. [CrossRef]
80. Gupta, H.; Chakrabarti, S.; Mothkuri, S.; Padya, B.; Rao, T.N.; Jain, P.K. High performance supercapacitor based on 2D-MoS_2 nanostructures. *Mater. Today Proc.* **2018**, *26*, 20–24. [CrossRef]
81. Huang, K.J.; Wang, L.; Liu, Y.J.; Wang, H.B.; Liu, Y.M.; Wang, L.L. Synthesis of polyaniline/2-dimensional graphene analog MoS_2composites for high-performance supercapacitor. *Electrochim. Acta* **2013**, *109*, 587–594. [CrossRef]